The activation of the metal-containing regulatory protein NiaR from *Thermotoga maritima* by its effector, nicotinic acid

Wai Chung Dorothy Cheng*[,1], Yuxin Li*[,1,2], Maileen Nakashima[1], Pierre Moënne-Loccoz[3], Katherine W. Rush[1,3,4] and Arthur Glasfeld[1^]

[1]Department of Chemistry, Reed College, Portland, Oregon, USA 97202

[2]Present address: Department of Biochemistry, Duke University School of Medicine, Durham, NC, USA 27710

[3]Department of Chemical Physiology and Biochemistry, School of Medicine, Oregon Health & Science University, Portland, Oregon, USA 97239

[4]Present address: Department of Chemistry and Biochemistry, Auburn University, Auburn, Alabama, USA 36849

*These authors contributed to the manuscript equally.

^Corresponding author: glasfeld@reed.edu

ORCID ID's of Authors

Wai Chung Dorothy Cheng	0000-0003-1545-0269
Yuxin Li	0000-0001-6593-1453
Maileen Nakashima	0009-0000-6488-3111
Pierre Moënne-Loccoz	0000-0002-7248-0873
Katherine W. Rush	0000-0001-6842-9055
Arthur Glasfeld	0000-0003-0680-0263

This version of the article has been accepted for publication, after peer review (when applicable) but is not the Version of Record and does not reflect post-acceptance improvements, or any corrections. The Version of Record is available online at: http://dx.doi.org/10.1007/s00775-025-02096-y. Use of this Accepted Version is subject to the publisher's Accepted Manuscript terms of use https://www.springernature.com/gp/open-research/policies/accepted-manuscript-terms.

Abstract

NiaR is a regulatory protein that represses the expression of proteins involved in the *de novo* biosynthesis and uptake of nicotinic acid (NA), with NA acting as a co-repressor. The previously published structure of NiaR from *Thermotoga maritima* (TmNiaR) identified it as a functional homodimer containing a transition metal ion in a suspected NA-binding pocket. Here, we present the crystal structure of NA bound to the iron-metalated form of TmNiaR. Supported by spectroscopic and solution studies, this structure shows that NA binds to a protein-bound ferrous ion via its ring nitrogen. Additionally, the carboxylate group on NA interacts with Tyr108 from the dyad-related subunit, repositioning the likely DNA-binding domains of the dimer to promote high-affinity interactions with DNA operators. The specificity of TmNiaR for NA can be explained by the hydrogen bonding scheme within the NA-binding pocket.

Keywords

Regulatory protein, metalloprotein, allostery, X-ray crystallography, XANES, resonance Raman spectroscopy

Abbreviations

NA	Nicotinic acid
XANES	X-ray absorption near edge spectroscopy
XAS	X-ray absorption spectroscopy
BhNiaR	Niacin repressor from *Bacillus halodurans*
TmNiaR	Niacin repressor from *Thermotoga maritima*

Introduction

Nicotinamide adenine dinucleotide (NAD) is essential in metabolism, serving as the primary biological cofactor for oxidation-reduction reactions and as a substrate for important enzymatic processes such as DNA ligation and ADP-ribosylation [1, 2]. In eubacteria, NAD synthesis uses nicotinic acid (NA; also referred to as vitamin B3 or niacin) as an intermediate. NA is produced by a *de novo* pathway from aspartic acid or obtained through a salvage pathway from exogenous sources or recycled NAD. Regulation of these approaches to generating NA for NAD biosynthesis is mediated by transcriptional regulatory proteins that use NA as a co-repressor [3].

One such protein, the niacin repressor (NiaR), has been characterized in a number of bacteria, including *Bacillus subtilis, Bacillus halodurans, Streptococcus pneumoniae*, and *Thermotoga maritima* [3–7]. NiaR represses the transcription of genes involved in the uptake or *de novo* synthesis of NA. Structures of NiaR from two sources have been reported. The ligand-free form of NiaR from *Thermotoga maritima* (TmNiaR) has been crystallized [7], as have the ligand-free and NA-bound forms of NiaR from *Bacillus halodurans* (BhNiaR) [5]. The two proteins share 39.5% sequence identity (Fig. S1a). Both structures reveal NiaR to be a functional homodimer, with each subunit containing an N-terminal domain (residues 1-63, *T. maritima* numbering) and a C-terminal domain (residues 71-172) joined by a flexible seven-residue linker (Fig. 1a). Dimerization is mediated by interactions between C-terminal domains, forming an eight-stranded β-sheet across the two subunits (Fig. S1b). The N-terminal domain contains a winged helix-turn-helix motif implicated in DNA binding. The C-terminal domain contains a bound transition metal that is part of the NA-binding pocket. In the dimeric structures of TmNiaR and BhNiaR, the C-terminal domains can be structurally aligned with a rmsd of 1.4 Å (measured between Cα atoms) indicating a relatively immobile core. In contrast the flexible linkers allow the N-terminal domains to adopt radically different positions with respect to that core (Fig. S2).

The metal-binding site in TmNiaR includes three histidine residues (His79, His146 and His148) and one glutamate residue (Glu87) that are also present in BhNiaR (Fig. S1a). In ligand-free TmNiaR, the unidentified metal ion is in a distorted octahedral coordination environment that includes a bound solvent molecule and bidentate interactions with Glu87 (Fig. 1b; [7]). In BhNiaR, the metal ion is identified as zinc, coordinated with tetrahedral geometry to His150, His152, and Glu91 in a monodentate interaction. In the ligand-free form, the fourth coordination position is occupied by a solvent molecule. His83 (equivalent to His79 in TmNiaR) is not part of the coordination sphere of the zinc ion. In ligand-bound BhNiaR, NA is bound to the zinc ion via its carboxylate group, replacing the water observed in the ligand-free form. The carboxylate also

forms a hydrogen bond to His83 (Fig. 1c; [5]).

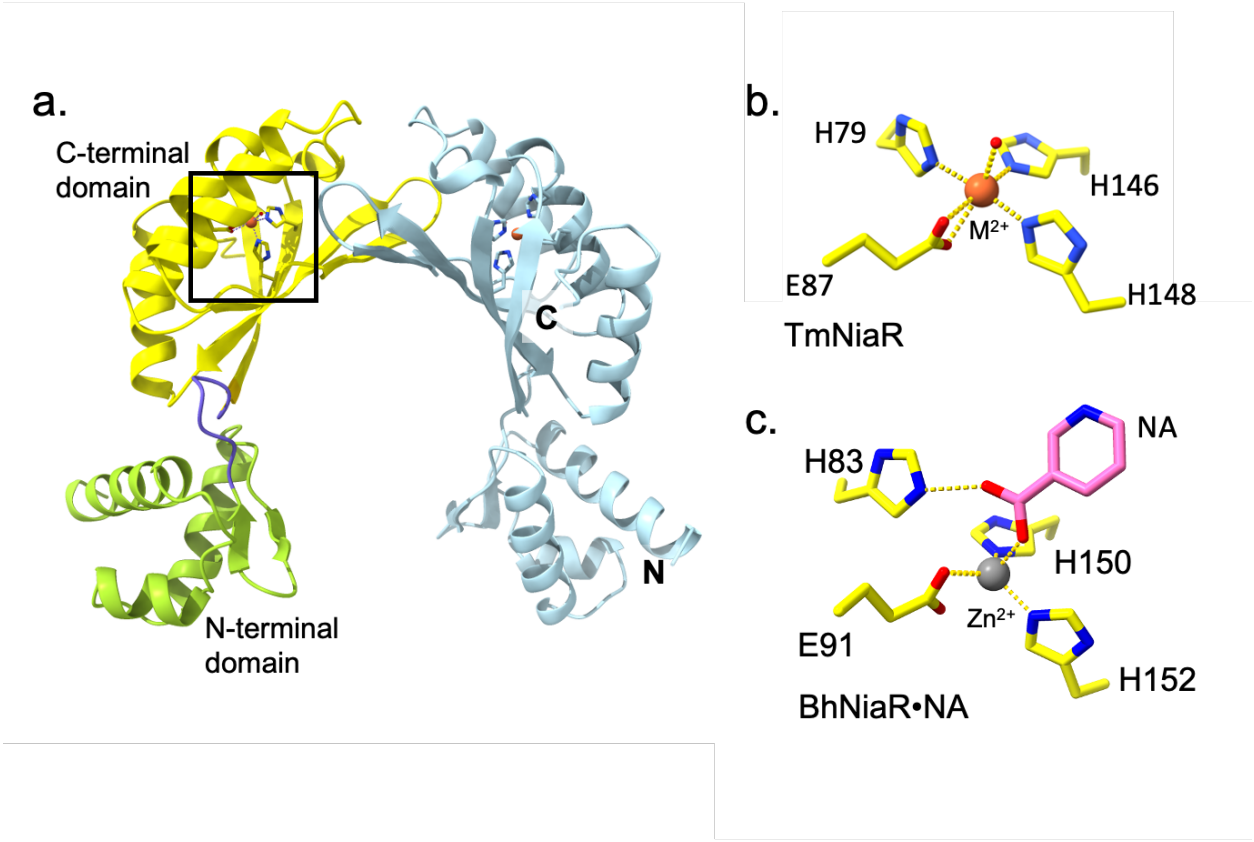

Fig.1 Published structures of NiaR: **a** Ribbon diagram of the TmNiaR dimer (PDB ID 1J5Y) [7]. The left-hand subunit is colored to show the N-terminal domain (light green), the C-terminal domain (yellow) and the linking peptide (dark blue). The N- and C-termini are labeled on the right-hand subunit. The metal binding site is boxed on the left-hand subunit and expanded in panel **b**; **c** The metal-binding site of BhNiaR including bound NA (PDB ID 7CV2) [5]

To date, the mechanism by which TmNiaR recognizes NA is unknown, and the identity of its bound metal ion is unresolved. While the structures of both ligand-free and NA-bound BhNiaR are reported, no significant changes in tertiary or quaternary structure are observed upon ligand binding, and BhNiaR is not in a conformation that permits DNA binding [5, 7]. Thus, no allosteric mechanism has been proposed for any NiaR protein. It also remains unclear whether the coordination geometry around the metal ion or other interactions with the bound co-repressor play a role in the mechanism of activation. To develop a molecular-level understanding of TmNiaR function, we have isolated TmNiaR homogeneously metalated with Fe^{2+} and have used structural, spectroscopic, and biochemical methods to define its interaction with NA and propose an allosteric mechanism for the activation of the protein to bind DNA.

Results

Metalation of TmNiaR

In the previous structural study performed on TmNiaR, the transition metal ion associated with the C-terminal domain was tentatively identified as Ni^{2+} [7]. Initial purification of TmNiaR from recombinant *E. coli* grown in Luria broth using a modified protocol revealed that the protein contained both iron and zinc (Table S1). To obtain homogeneous samples of iron-bound TmNiaR, subsequent purifications were performed using protein expressed in *E. coli* grown in minimal media supplemented with ferric ammonium citrate. X-ray absorption spectroscopy (XAS; see below) indicated that the iron associated with TmNiaR was in the Fe(II) oxidation state. Using the absorbance at 205 nm, calibrated to amino acid analysis, to measure protein concentration [8], we determined that TmNiaR isolated from *E. coli* grown in supplemented M9 medium was ≥ 90% metalated with iron as determined by ICP-OES (Table S1).

NA interacts with TmNiaR by coordinating Fe^{2+} via its ring nitrogen

TmNiaR•Fe^{2+} was successfully crystallized in complex with NA (Fig. 2, Table 1). X-ray fluorescence spectroscopy conducted at the beamline confirmed the presence of iron in the crystal (Fig. S3). A model of TmNiaR•Fe^{2+} bound to NA was obtained by molecular replacement, and the structure was refined to 2.3 Å resolution. The final model includes a single subunit of TmNiaR in the asymmetric unit, along with nine solvent molecules, an Fe^{2+} ion, NA and a bound molecule of L-proline from the crystallization solution. The model lacks five N-terminal residues and two C-terminal residues.

The domain architecture of the TmNiaR•Fe^{2+}•NA complex mirrors that of ligand-free TmNiaR. The N-terminal domain (residues 6-63) features a winged helix-turn-helix motif, previously identified by Weekes et al. [7] as responsible for DNA binding. The C-terminal domain with an α/β fold (residues 71-173) contains the Fe^{2+} ion and a bound NA molecule. The structures of the N-terminal domains of ligand-free and ligand-bound TmNiaR overlap with a rmsd of 0.28 Å (measured between α-carbons of residues 6-63) while the C-terminal domains align with a rmsd of 0.43 Å between the α-carbons of residues 71-173. The two domains are connected by a linker (residues 64-70), which adopts a more extended conformation in the NA-bound structure compared to ligand-free TmNiaR or BhNiaR. This extension results in a greater separation between the DNA-binding domains in the NA-bound form (Fig. 2a).

Table 1 Data collection and refinement statistics for the TmNiaR•NA complex (PDB ID: 9EBR)[a]

Data Collection Statistics	
Wavelength (Å)	0.9795
Space group	$P3_221$
Unit cell a,b,c axes (Å)	83.24, 83.24, 66.84
Resolution range (Å)	35.33 - 2.30 (2.38 - 2.30)
Total reflections	121789 (11886)
Unique reflections	12235 (1190)
Multiplicity	10.0 (10.0)
Completeness (%)	100.0 (100.0)
$\langle I/\sigma(I) \rangle$	35.5 (3.7)
Wilson B-factor	65.89
R_{meas}	0.032 (0.559)
R_{pim}	0.014 (0.243)
$CC_{1/2}$	1.000 (0.935)
Refinement statistics	
Reflections used in refinement	12204 (1207)
Reflections used for R_{free}	614 (66)
R_{work}	0.2168 (0.3603)
R_{free}	0.2596 (0.3836)
Number of non-hydrogen atoms	1347
macromolecules	1328
ligands	14
solvent	9
Protein residues	169
RMS bonds (Å)	0.008
RMS angles (°)	0.98
Ramachandran favored (%)	97.0
Ramachandran allowed (%)	3.0
Ramachandran outliers (%)	0.0
Average B-factor (Å^2)	86.35
macromolecules	86.63
ligands	66.06
solvent	68.50
Number of TLS groups	6

[a]Statistics for the highest-resolution shell are shown in parentheses.

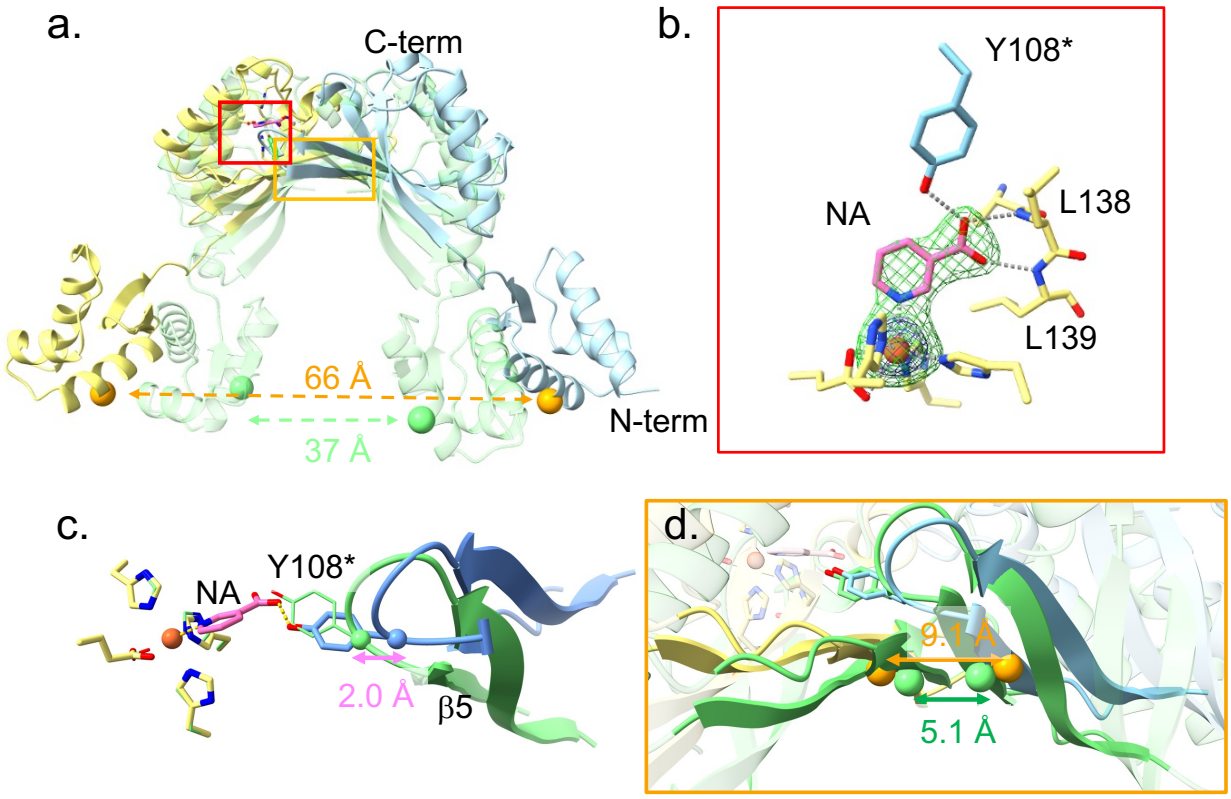

Fig. 2 Crystal structure of TmNiaR•Fe^{2+} in complex with NA **a** Symmetric structural alignment of the NA-bound TmNiaR dimer (subunits colored yellow and cyan; PDB ID 9EBR) atop the ligand-free TmNiaR dimer (light green; PDB ID 1J5Y). The DNA-binding domains in NA-bound TmNiaR are positioned further apart than in the ligand-free form (66 Å vs. 37 Å), as measured from the C_α atoms of Gln43 (spheres) in the recognition helix; **b** NA-binding pocket in TmNiaR (red box in **a**). Omit F_{obs}-F_{calc} electron density maps, with NA and Fe^{2+} at zero occupancy, are shown in green (at 5.5 σ) and blue (12 σ). NA (pink carbons) binds the Fe^{2+} ion via its ring nitrogen, while its carboxylate forms hydrogen bonds with Tyr108* (cyan carbons) and the amide nitrogens of Leu138 and Leu139; **c** Structural alignment of the NA-bound TmNiaR metal-binding site on that of ligand-free TmNiaR. Coloring of carbon atoms as in **a**. The metal binding geometry is unaltered between the two forms, with the ring nitrogen of NA occupying the same position as the Fe^{2+}-bound water in the ligand-free form. The movement of Tyr108* leads to a 2.0 Å displacement of its α-carbon, impacting the position of β-strand 5. **d** Close-up of the boxed region from **a** highlighting the linkage of movement in the α-carbon of Tyr108* to the spreading of the dyad-related β-strands 5 from 5.1 Å to 9.1 Å. The distances are measured from the α-carbons of Arg112, depicted as spheres, on each strand.

Bound NA is coordinated via its ring nitrogen to the Fe^{2+} ion (Fig. 2b). The protein coordination geometry around Fe^{2+} in the NA-bound form is identical to that in ligand-free TmNiaR, with three histidine residues (His79, His146 and His148) and a bidentate carboxylate from Glu87. The ring nitrogen of NA replaces the metal-bound solvent molecule in the ligand-free structure [7]. Additional contacts between NA and TmNiaR are made via van der Waals interactions with non-polar residues lining the binding pocket (Ile84, Leu88, Phe126, Met130 and Leu139) and via hydrogen-bonds to the carboxylate group of NA (Fig. 2b). Those hydrogen bonds are donated by the backbone amide groups of Leu138 and Leu139, which are part of a flexible loop that shifts ~2.5 Å closer to NA in the bound state, and the phenolic hydroxyl group of Tyr108* from the dyad-related subunit of the dimer (the dyadic relationship is indicated with "*"). In the NA-bound conformation, Tyr108* is 2.0 Å further away from the metal ion compared to its position in the ligand-free structure (Fig. 2c).

This shift impacts the structure of the dimer interface (Fig. 2d). Tyr108 resides in a β-turn linking β-strands 4 and 5 (residues 97-114), which form the core of the eight-stranded β-sheet spanning both subunits of ligand-free TmNiaR (Fig. S1b). In the NA-bound form, the movement of Tyr108 disrupts the hydrogen bonds between the two central β-strands (dyad-related strands 5, residues 109-114), causing the central β-strands to separate by approximately 4 Å, as measured between the α-carbons of Arg112 on the two strands (Fig. 2d). This conformational change causes the C-terminal domains of the dimer to spread apart, while the linker peptide connecting the N-terminal DNA-binding domain to the C-terminal domain becomes more extended. As a result, the separation between the N-terminal DNA-binding domains increases significantly, from 37 Å to 66 Å, as measured between the dyad-related Gln43 residues on the recognition helix (Fig. 2a).

These observations suggest a plausible mechanism for a conformational change in TmNiaR upon binding NA. However, given that the metal-ion coordination geometry and NA-binding schemes observed in TmNiaR are different than those described in BhNiaR, further studies were conducted to confirm the octahedral coordination of Fe^{2+} and its interaction with the ring nitrogen of NA in solution.

X-ray absorption spectroscopy indicates Fe^{2+} is in hexacoordinate geometry

The X-ray absorption near edge structure (XANES) region of the Fe K-edge spectrum contains information about the Fe oxidation state and coordination geometry [9–11], and has been used

in the characterization of many Fe^{2+} protein active sites (for relevant examples [12–14]). X-ray absorption spectroscopy was used to confirm the oxidation state of the bound iron and to explore the geometry of the coordination sphere around the Fe^{2+} ion in the presence and absence of NA (Fig. 3). As radiation damage and photoredox processes can lead to perturbations in X-ray absorption data, particularly for potential higher valent species (Fe^{3+}), the first and second scans of each sample revealed no changes due to radiation exposure (Fig. S4).

The Fe K-edge XANES spectrum of NiaR in the absence of NA is characteristic of octahedral Fe^{2+} with a low intensity pre-edge feature arising from 1s → 3d transitions and a maximum edge intensity at 7127 eV (Fig. 3, black line). Upon the addition of NA, the spectrum is effectively unchanged (Fig. 3, red line), indicating that ligand binding induces no major changes to the Fe^{2+} coordination environment, consistent with the observation that, in the crystal structures of ligand-free [7] and ligand-bound TmNiaR, there is little change in the position of the atoms coordinating the metal ion. A tetrahedral Fe^{2+} coordination environment as seen in the Zn^{2+} BhNiaR structure can be ruled out, as such spectra are characterized by a lower energy spectral maximum and a significantly larger pre-edge peak area that correlates with coordination number [10, 11].

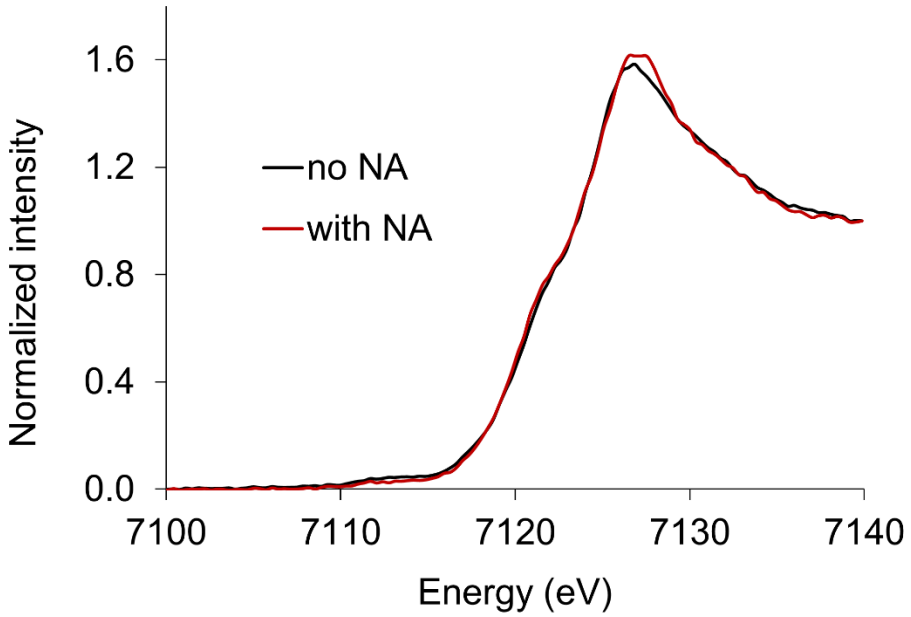

Fig. 3 TmNiaR Fe K-edge XANES spectra in the presence and absence of NA. Only subtle changes in the spectra are seen and the edge positions, edge maxima, and pre-edge intensities remain constant. The total pre-edge peak areas were determined to be 5.3 x 10^{-2} eV (without

NA) and 5.1 x 10^{-2} eV (with NA), which are consistent with the cited examples of octahedral Fe^{2+} coordination environments in the literature [10, 11]. Fits can be found in Fig. S5.

Resonance Raman Spectroscopy indicates NA is bound to Fe^{2+} via its nitrogen

In preparing concentrated (>500 µM) samples of TmNiaR•Fe^{2+} for XAS analysis and X-ray diffraction, we noticed that the pale green color of the protein solution turned a bright yellow color upon addition of NA (Fig. S6), which corresponds to the appearance of an absorption peak at 430 nm (Fig. 4). A comparable absorption band was obtained when pyridine was added to TmNiaR solutions, but not with benzoic acid, suggesting that the interaction between NA and Fe^{2+} gives rise to a metal to ligand charge transfer (MLCT) via nitrogen coordination to the metal ion.

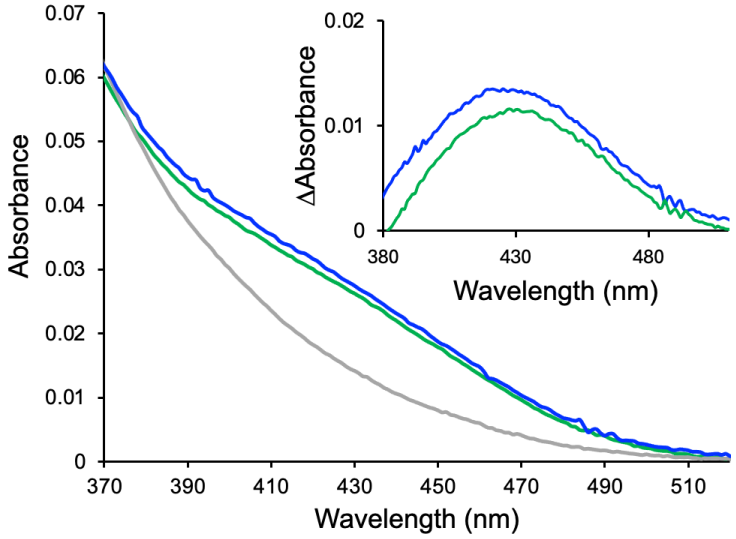

Fig. 4 UV/Vis spectra of 50 µM ligand-free TmNiaR•Fe^{2+} (grey curve) and TmNiaR•Fe^{2+} in a solution of 100 µM nicotinic acid (blue curve) or 100 µM pyridine (green curve). Inset shows the difference spectra of ligand-bound forms vs. the ligand-free form of TmNiaR•Fe^{2+}

Resonance Raman spectroscopy was used to confirm the structural origin of the visible absorbance centered at 430 nm, and to provide evidence that the NA-binding mode observed in the crystal structure also occurs in solution at room temperature. Resonance Raman spectra of TmNiaR were collected in its ligand-free form or with pyridine or NA, and with perdeuterated forms of those ligands (Fig. 5). The Raman spectrum of ligand-free TmNiaR exhibits pre-resonance vibrations from aromatic sidechains and amide backbone vibrations, including the bands at around 1600-1690 cm^{-1} (amide I), 1400-1490 cm^{-1} (CH), and 1230-1300 cm^{-1} (amide III) [15, 16]. The addition of pyridine or NA results in the appearance of a large number of

resonance-enhanced ring vibrations in the high and mid-frequency region that shift upon ligand deuterations (from d_5-pyridine and d_4-NA; Table S2). None of these resonance enhanced signals are observed with 568- or 407-nm laser excitations, supporting an assignment of the absorption features centered at 430 nm to Fe(II) → pyridine or Fe(II) → NA, to MLCT transitions.

Although there have been no prior reports of resonance Raman studies on Fe(II)-NA complexes, almost all the characteristic bands presented with the TmNiaR-pyridine complex are within a few wavenumbers from the frequencies described previously for the $(Py)_2$Fe(II)MP complex (Py = pyridine, MP = mesoporphyrin IX dimethyl ester) as well as other metal(Py) complexes (Table S2) [17, 18]. In addition, the overall distribution of resonance enhanced vibrational modes are similar for the addition of pyridine and NA ligands. We may thus conclude that both ligands have a conserved N-atom ligation to Fe(II). Unfortunately, a distinct Fe(II)-N(Py) or Fe(II)-N(NA) stretching vibration expected between 200-300 cm^{-1} does not appear to be resonance-enhanced and cannot be distinguished from the non-resonant Raman background of the protein.

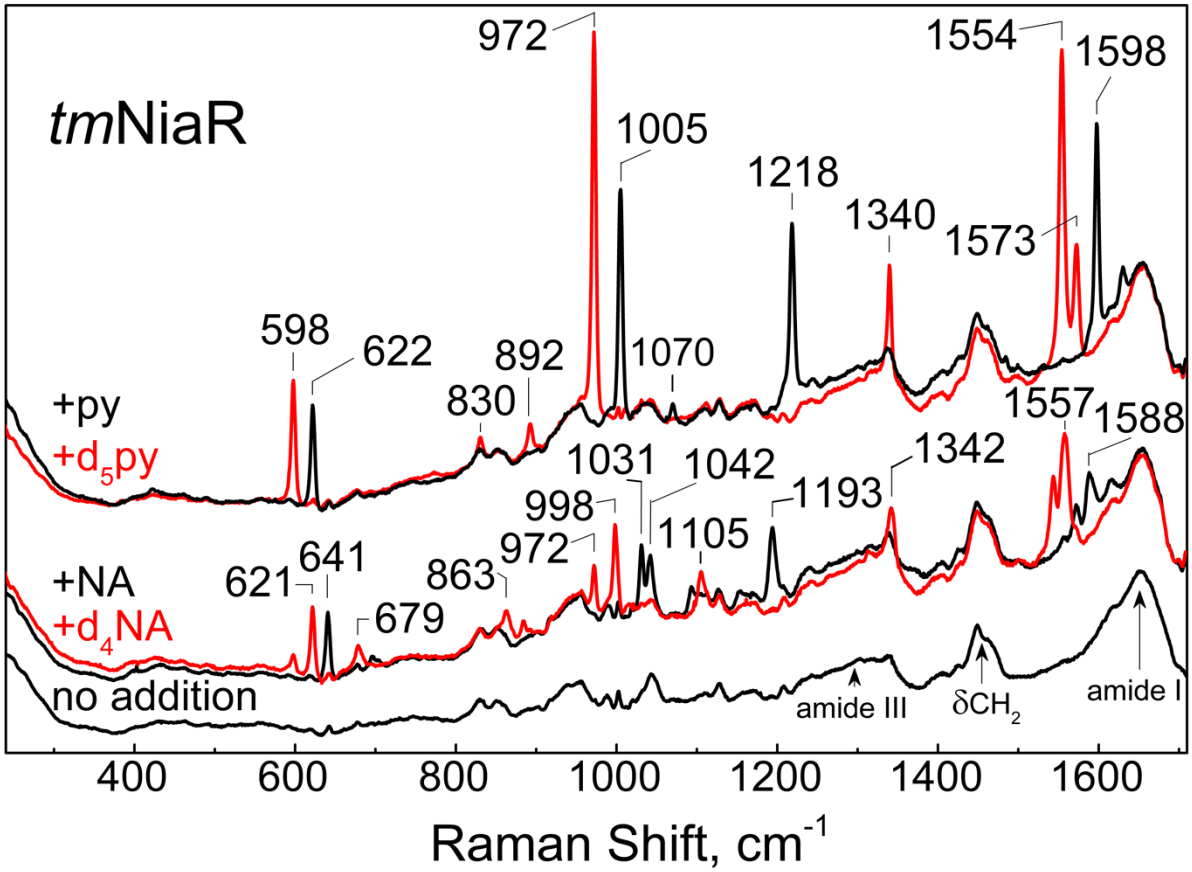

Fig. 5 Room-temperature resonance Raman spectra of TmNiaR obtained with a 442-nm laser excitation in the absence of added ligand (bottom black trace), after the addition of NA (middle traces, unlabeled NA (black trace) and deuterated NA (red trace), and after the addition of pyridine (Py) (top traces, unlabeled Py (black trace) and deuterated Py (red trace))

TmNiaR is selectively activated by NA

The structure of TmNiaR•Fe^{2+}•NA suggests that TmNiaR can exert selectivity for NA over structurally related compounds via the geometry of hydrogen bonding to the carboxylate group of NA. To probe this selectivity, we took advantage of the metal-to-ligand charge transfer band at 430 nm to measure the affinity of TmNiaR•Fe^{2+} for NA and two analogs: pyridine and nicotinamide (Fig. 6). Analysis of the binding data revealed that NA appears to bind with significant negative cooperativity. In comparing models for one NA molecule binding per subunit vs one NA molecule per dimer, the latter gives a significantly better fit (Fig. 6). Nevertheless, a TmNiaR dimer can bind NA in both subunits. Modeling NA at 0.5 occupancy in the structure

revealed strong positive density in the F_{obs}-F_{calc} map (Fig. S7), indicating full occupancy of NA at each subunit. For pyridine and nicotinamide, no significant difference in fit between the two stoichiometries of binding was observed. The binding affinities for the three ligands reveals a clear ranking. NA binds too tightly to give a quantitative measure of affinity under our assay conditions ($K_d \leq 3$ μM assuming 1:1 NA:dimer), while pyridine binds with 22 ± 15 μM affinity (assuming 1:1 NA:subunit) and nicotinamide very weakly (K_d >1 mM assuming 1:1 nicotinamide:subunit).

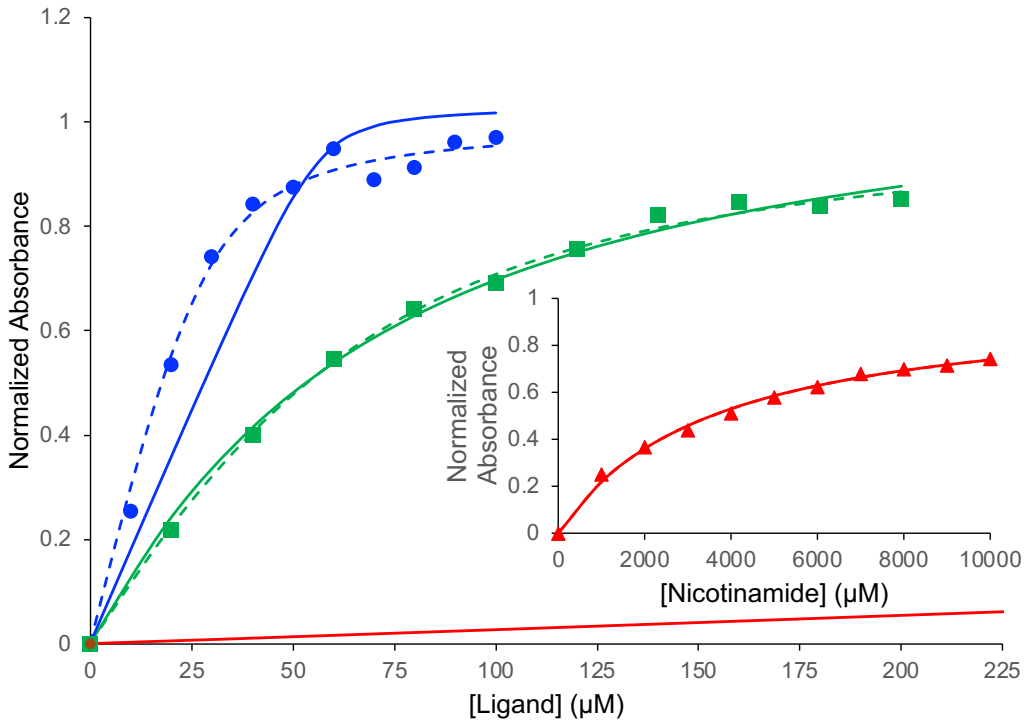

Fig. 6 Titrations of TmNiaR with NA, pyridine, and nicotinamide. Titrations were monitored by absorbance at the respective maximum wavelengths for NA (blue circles), pyridine (green squares), and nicotinamide (inset; red triangles). Solid lines represent fits to the data assuming a 1:1 binding stoichiometry of the ligand to each subunit of TmNiaR, while dashed lines represent fits assuming a 1:1 binding stoichiometry of the ligand to the dimer. The two fits overlap without visible difference for the nicotinamide titrations.

While NA, pyridine and nicotinamide all bind to TmNiaR•Fe^{2+}, they do not uniformly activate the protein for DNA binding, as assayed using fluorescence anisotropy and a fluorescein-labeled duplex DNA containing the *nadB* operator sequence. The ligand-free protein shows weak, non-

specific association with duplex DNA under the assay conditions (Fig. 7). At 1 mM concentration, NA activates TmNiaR for DNA binding, with a dissociation constant of 210 ± 20 nM (N=3). At the same concentration, nicotinamide does not observably activate TmNiaR. However, the pyridine complex of TmNiaR•Fe^{2+} appears to abolish the weak DNA binding observed with the ligand-free protein. To further investigate the importance of the ring nitrogen in coordinating the ferrous ion, we tested the ability of 1 mM benzoic acid to activate TmNiaR. The presence of benzoic acid did not influence the association of TmNiaR with DNA, indicating the that the ring nitrogen plays a crucial role in the activation mechanism (Fig. 7).

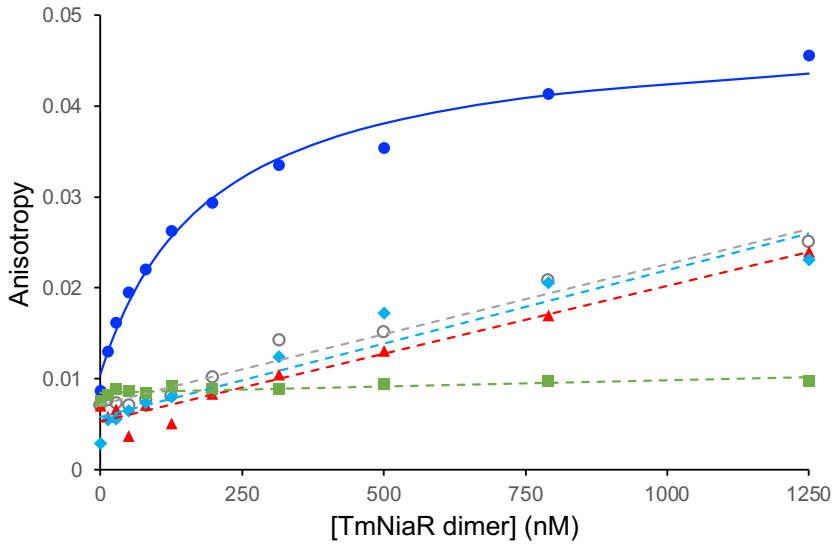

Fig. 7 Activation of TmNiaR for DNA binding by NA and analogs, as assayed using fluorescence anisotropy. Representative titrations of a fluoresceinated DNA duplex containing the *nadB* operator sequence with TmNiaR in the absence or presence of 1 mM ligand, as monitored by fluorescence anisotropy. NA (blue circles) activates TmNiaR to bind DNA at 50˚C. The solid blue line indicates the fit of the data to a 1:1 binding isotherm yielding a K_d of 210 ± 20 nM (N=3), while weak non-specific binding is observed in the absence of any ligand (open grey circles) or with nicotinamide (red triangles) and benzoic acid (light blue diamonds). The presence of 1 mM pyridine (green squares) appears to block the non-specific binding of TmNiaR to the DNA duplex. Dotted lines are linear regressions to show the trend in the data, colored according to the ligand described above

Discussion

We successfully isolated TmNiaR recombinantly expressed in *E. coli*, homogeneously metalated with Fe^{2+}, and have solved the crystal structure of this protein bound to its effector, NA. Leveraging the spectral properties of the Fe^{2+} ion, we confirmed the mode of NA binding to the repressor and propose a mechanism of activation consistent with both structural and biochemical evidence.

Previous studies on BhNiaR, a homolog of TmNiaR, isolated with a bound Zn^{2+} ion, showed that NA binds to the metal ion and His83 via its carboxylate without forming additional specific contacts to the protein [5]. In contrast, the structure of iron-metalated TmNiaR shows NA bound to the metal ion via its ring nitrogen. This binding geometry is confirmed by resonance Raman spectroscopy, which uses the MLCT band arising from the nitrogen-Fe^{2+} bond to reveal vibrational modes associated with the pyridine ring. Another key difference between the structure of TmNiaR•NA and BhNiaR•NA is the coordination geometry of the metal ion. The Zn^{2+} ion in BhNiaR is bound in tetrahedral geometry, excluding a conserved histidine (His83, which is His79 in TmNiaR numbering) from the coordination sphere. The Fe^{2+} ion of TmNiaR binds quite differently, with distorted octahedral geometry that includes ligation by His79 in both the ligand-free and NA-bound forms. X-ray absorption spectroscopy confirms the persistence of octahedral geometry in solution, removing a possible mechanistic linkage between coordination geometry and activation by NA binding. Interestingly the same metal ion geometry was observed in the original structure solved by Weekes et al. [7] from TmNiaR purified from *E.* coli without an effort to selectively metalate it.

Despite the availability, from *E. coli* expression systems, of TmNiaR homogeneously metalated with iron and BhNiaR metalated with zinc [5], the native metal ions for both proteins remains uncertain. The native metalation state of a protein depends on both the affinity of the protein for different metal ions as well as the availability of those ions in the native host cell, which can vary from those found in *E. coli* [19]. Further experimentation will be needed to confirm the native metal for both TmNiaR and BhNiaR. However, some metalloproteins function comparably with iron and zinc [20, 21], so the differences observed between TmNiaR and BhNiaR might be imposed by differences in protein structure, rather than the identities of the bound metal.

In any case, the results reported here strongly support a mechanism for the activation of TmNiaR•Fe^{2+} by NA. The Fe^{2+}-bound NA is positioned so that its carboxylate accepts three

hydrogen bonds: two from the backbone amide nitrogens of Leu138 and Leu139, and one from phenolic hydroxyl group of Tyr108*, contributed by the 2nd subunit of the homodimeric repressor. To interact with bound NA, Tyr108* shifts approximately 2.0 Å relative to the ligand-free conformation of NiaR, disrupting the β-sheet spanning the dimer interface in ligand-free NiaR and altering the relative positioning of the two subunits. These structural changes presumably permit the DNA-binding domains of NiaR to adopt the necessary positions for high-affinity operator binding.

In support of this mechanism, neither benzoate nor pyridine activates TmNiaR for DNA binding. Benzoate cannot interact with the transition metal due to the absence of a ring nitrogen. Pyridine, which binds to Fe^{2+} via its ring nitrogen as confirmed by resonance Raman spectroscopy, instead disrupts the weak, non-specific DNA binding observed in ligand-free TmNiaR. This suggests that the presence of pyridine in the co-repressor binding site prevents the conformational changes necessary for DNA-binding activity. Similarly, nicotinamide binds less strongly than NA, because its amide group is not well accommodated by the hydrogen bond donors in TmNiaR, and it fails to activate the protein at 1 mM concentration. The observed negative cooperativity of NA binding suggests that, in its functional cellular state, TmNiaR may bind only one NA molecule may bind per dimer. However, the ligand-binding selectivity observed in solution at micromolar NA concentrations aligns with the spectroscopic, DNA-binding, and structural results obtained at millimolar NA concentrations.

The proposed mechanism for TmNiaR activation by NA is consistent with the combined structural and solution-based analyses presented here. Further studies on TmNiaR and BhNiaR, as well as NiaR homologs from other species, could reveal a shared mechanistic framework for NiaR function across bacterial species.

Methods

Expression and Purification of TmNiaR

A synthetic gene for TmNiaR, codon optimized for expression in *E. coli*, was obtained (Genscript) and cloned into the pSMT3 plasmid [22] such that TmNiaR was expressed as a fusion with an N-terminal hexahistidine-tagged SMT3 domain. The construct was designed to yield an N-terminal methionine on TmNiaR following cleavage with Ulp protease. Expression of the fusion protein was performed in *E. coli* NiCo21(DE3) cells (New England Biolabs) in Luria broth, or in M9 minimal media supplemented with 0.2 g/L ferric ammonium citrate to achieve homogeneous metalation with iron. Expression was induced with 0.5 mM IPTG and cells continued to grow at 2-3 hours at 37˚C in Luria broth or overnight at 20˚C in minimal media before harvesting.

TmNiaR was purified using solutions containing either HEPES or sodium phosphate buffers as follows, with "buffer" indicating that both buffering agents were used in otherwise identical formulations. Cells were lysed by sonication in buffer A (25 mM buffer, pH 7.5, 300 mM sodium chloride) with 10 mM imidazole. The extract was loaded onto a Talon cobalt ion affinity column and the fusion protein was eluted with a 10-300 mM gradient of imidazole in buffer A. The fusion protein was cleaved by the addition of Ulp protease during an overnight dialysis step against buffer A containing 10 mM imidazole and 1 mM β-mercaptoethanol. TmNiaR was isolated in the flow through after the dialysate was loaded onto a nickel ion affinity column, while the protease and STM3 domain, both containing hexahistidine tags, were retained by the column. Protein was dialyzed against buffer B (25 mM buffer, pH 7.5, 100 mM NaCl) and concentrated and stored at -80˚C. Because TmNiaR does not have any native tryptophan residues, the absorbance of the protein at 205 nm [8] was used to measure concentration in buffer B containing sodium phosphate, using a extinction coefficient of 4.6×10^5 $1/M \cdot cm$, as validated by amino acid analysis (Molecular Structure Facility, University of California, Davis). Metal ion determination was performed by ICP-OES following dilution of concentrated protein samples into a matrix of 0.1% nitric acid. ICP-MS measurements were performed by the Elemental Analysis Core Facility at Oregon Health and Sciences University.

Crystallization and X-ray diffraction data collection

Crystals of the TmNiaR•Fe^{2+}•NA complex were obtained by hanging drop co-crystallization of the protein (10 mg/mL in buffer B with sodium phosphate) with 1 mM NA against a well solution of 0.2 M L-proline, 0.1 M HEPES pH 7.5, and 10% (*w/v*) PEG 3350. Diffraction data were collected using synchrotron radiation at beamline 9-2 at the Stanford Synchrotron Radiation Lightsource (SLAC National Accelerator Laboratory, CA) from crystals that had been transferred to paratone-N or solutions containing 10% to 30% ethylene glycol in addition to the well solution components and then flash cooled in liquid nitrogen.

Structure solution and refinement were performed using the PHENIX suite of crystallographic software [23], and modeling was performed using Coot [24]. The structure of TmNiaR bound to NA was solved by molecular replacement on the individual domains in Phaser [25] using the ligand-free form of TmNiaR (PDB 1J5Y) as a search model [7]. Structural models were iteratively built and refined in Coot and phenix.refine. Figures were generated using the computer program *ChimeraX* [26]. The model and structure factors have been deposited with the Protein Data Bank (9EBR).

Ligand binding assays

Binding of ligands to TmNiaR•Fe^{2+} was monitored by absorbance measurements recorded on an Agilent Cary 60 UV-visible spectrophotometer using sub-micro quartz cell of 1 cm path length. Titrations of 57 μM TmNiaR•Fe^{2+} in phosphate-containing buffer A were performed by addition solutions of potential ligands, including NA, nicotinamide and pyridine while monitoring absorbance at 430 nm which arises from a metal to ligand charge transfer band between the bound Fe^{2+} and ligated ligand containing a pyridine ring. Data were fit to 1:1 binding models using *Dynafit* software [27].

DNA binding assays

The activation of TmNiaR was measured using a fluorescence anisotropy-based DNA-binding assay. A 23-base oligodeoxynucleotide (Integrated DNA Technologies) with the sequence TTGTTTACAGCAGGTGTAAACTT, which contains the *nadB* operator sequence, and a 5'-carboxyfluorescein label was annealed with a 10% molar excess of its unlabeled complement in buffer (25 mM HEPES, 50 mM NaCl, pH 7.5) by heating to 90°C and then slowly cooled to room temperature, creating a DNA duplex containing a single fluorescent label. The DNA-binding activity was measured by titrating solutions of ~20 μM TmNiaR dimer into 1 mL of solution

containing 1 nM of labeled DNA in FA buffer (25 mM HEPES, pH 7.5, 300 mM NaCl) in the presence of a fixed concentration (1 mM) of ligand at 50˚C. Anisotropy was measured on a Beacon 2000 fluorescence polarization instrument (Panvera LLC, Madison, WI). Data were analyzed assuming a 1:1 binding stoichiometry between the *TmNiaR* dimer and labeled DNA using equation 1:

$$r = \Delta r \left(\frac{[P]}{[P]+K_d}\right) + r_{min} \qquad \text{(Eq. 1)}$$

where *r* is the measured anisotropy, Δr is the maximum observed change in anisotropy and r_{min} is the anisotropy of unbound DNA. [P] is the total concentration of protein dimers, and K_d is the dissociation constant of NiaR from the duplex DNA.

X-Ray absorption near edge structure (XANES) data collection

Samples were prepared using ~1.5 mM TmNiaR•Fe^{2+} in 25 mM HEPES buffer pH 7.5 with 100 mM NaCl and 10% glycerol, and 2 mM ligand concentration when present. Each sample was mixed with 20% (*v/v*) ethylene glycol and measured as frozen glasses at 10 K.

X-ray data collection was conducted as described by Rao et al. [28]. Fe K-edge (7111 eV) X-ray absorption measurements were made at beamline 7-3 of the Stanford Synchrotron Radiation Lightsource (SSRL) operating at 500 mA current in continuous top-off mode. Beamline 7-3 is equipped with a Si[220] monochromator with a ϕ = 90° crystal set, which was detuned 50% to reject harmonic wavelengths. Fe Kα fluorescence was collected using a 30-element Canberra Ge array detector. A Z-1 (Mn) metal oxide filter and Soller slit assembly was installed in front of the detector to attenuate the contribution of elastic scattering. Data are averages of 2 scans and a buffer blank was subtracted from the raw data to produce a flat pre-edge and eliminate residual Mn fluorescence arising from the metal oxide filter. An Fe metal foil was placed between the second and third ionization chamber to facilitate energy calibration by setting the first inflection point of the foil absorbance feature to 7111.0eV.

XAS data averaging, background subtraction, and normalization were performed using the PROCESS module of EXAFSPAK [29]. Data were normalized to the edge jump and pre-edge peak areas were determined using the EDG_FIT least-squares fitting module of EXAFSPAK. The pre-edge region (7106-7118 eV) was fit by a combination of a pseudo-Voigt background function and pseudo-Voigt peak functions representing the pre-edge transitions. All pseudo-

Voigt functions were comprised of a 50% Lorentzian component, which accounts for broadening arising from the 1s core-hole lifetime, and a 50% Gaussian component. The best fits, as determined by lowest RMSD, included two pre-edge peaks centered around 7112 eV and 7113 eV, as has been established in the literature [11]. The pre-edge peak functions determined from the fitting result were integrated to yield the pre-edge peak area.

Resonance Raman Spectroscopy

Samples in 25 mM HEPES buffer pH 7.5 with 100 mM NaCl were prepared in Raman capillaries using ~2 mM protein solution and 2.5 mM ligand concentration when present. All spectra were collected at room temperature using a 442-nm laser excitation.

Resonance Raman spectra were obtained on a custom McPherson 2061/207 spectrograph set at 0.67 m with 1800 grooves per mm holographic grating and equipped with a liquid-nitrogen-cooled CCD detector (LN-1100 PB, Princeton Instrument). The 442 nm excitation laser was obtained from a HeCd laser (Liconix, Santa Clara CA). The 300-1800 cm^{-1} spectral range was achieved by collecting two different windows with sufficient overlap in the 1000 cm^{-1} region to match relative intensities between high and low-frequency spectra. High quality RR spectra were obtained using 10-min total acquisition time with 15 mW laser power per spectral window. Resonance enhancement conditions with the 442 nm laser excitation were confirmed by collecting spectra with the 407 and 568 nm excitations from a Kr laser (Innova 302C, Coherent). Long-pass filters (RazorEdge, Semrock) were used to attenuate the Rayleigh scattering. The RR spectra were collected in a 90° scattering geometry on samples mounted on a reciprocating translation stage. Frequencies were calibrated relative to indene and are accurate to ± 1 cm^{-1}. Polarization conditions were optimized using CCl_4 and indene. The integrity of the RR samples was confirmed by direct monitoring of their UV-vis absorption spectra in Raman capillaries before and after laser exposure. The lack of photosensitivity of the samples was confirmed by comparing rapid acquisitions within a range of laser powers and continuous sample translation with longer data acquisitions on static samples.

Acknowledgements

The authors wish to thank Danielle Cass and Shivani Ahuja (Reed College) for helpful conversations and assistance. Thanks to Ninian Blackburn (Oregon Health & Science University) for generously allowing the use of his ICP-OES instrument and to Dr. Sinan Sabuncu

(Oregon Health & Science University) for assistance with early Resonance Raman experiments. Use of the Stanford Synchrotron Radiation Lightsource, SLAC National Accelerator Laboratory, is supported by the U.S. Department of Energy, Office of Science, Office of Basic Energy Sciences under Contract No. DE-AC02-76SF00515. The SSRL Structural Molecular Biology Program is supported by the DOE Office of Biological and Environmental Research, and by the National Institutes of Health, National Institute of General Medical Sciences (including P41GM103393). The contents of this publication are solely the responsibility of the authors and do not necessarily represent the official views of NIGMS or NIH.

Statements and Declarations

Author Contributions

All authors contributed to the study conception and design, material preparation, data collection and analysis. AG supervised the studies. The first draft of the manuscript was written by AG, PM-L and KR, and all authors commented on previous versions of the manuscript. All authors read and approved the final manuscript.

Funding

Reed College provided funding to support this work.

Data Availability

The model and structure factors of the TmNiaR•Fe^{2+}•NA complex have been deposited with the Protein Data Bank (9EBR). Other datasets generated and/or analyzed during the study are not publicly available because they have not been uploaded to any public repository but are available from the corresponding author on reasonable request.

Conflict of Interest

The authors declare no relevant financial or non-financial competing interests.

Ethics approval and consent to participate

Not applicable.

Consent for publication

Not applicable

References

1. Wilkinson A, Day J, Bowater R (2001) Bacterial DNA ligases. Molecular Microbiology 40:1241–1248. https://doi.org/10.1046/j.1365-2958.2001.02479.x

2. Ziegler M (2000) New functions of a long-known molecule. European Journal of Biochemistry 267:1550–1564. https://doi.org/10.1046/j.1432-1327.2000.01187.x

3. Rodionov DA, Li X, Rodionova IA, et al (2008) Transcriptional regulation of NAD metabolism in bacteria: genomic reconstruction of NiaR (YrxA) regulon. Nucleic Acids Res 36:2032–2046. https://doi.org/10.1093/nar/gkn046

4. Rossolillo P, Marinoni I, Galli E, et al (2005) YrxA Is the Transcriptional Regulator That Represses De Novo NAD Biosynthesis in Bacillus subtilis. J Bacteriol 187:7155–7160. https://doi.org/10.1128/JB.187.20.7155-7160.2005

5. Lee DW, Park YW, Lee MY, et al (2020) Structural analysis and insight into effector binding of the niacin-responsive repressor NiaR from Bacillus halodurans. Sci Rep 10:21039. https://doi.org/10.1038/s41598-020-78148-x

6. Afzal M, Kuipers OP, Shafeeq S (2017) Niacin-mediated Gene Expression and Role of NiaR as a Transcriptional Repressor of niaX, nadC, and pnuC in Streptococcus pneumoniae. Front Cell Infect Microbiol 7:70. https://doi.org/10.3389/fcimb.2017.00070

7. Weekes D, Miller MD, Krishna SS, et al (2007) Crystal structure of a transcription regulator (TM1602) from Thermotoga maritima at 2.3 Å resolution. Proteins: Structure, Function, and Bioinformatics 67:247–252. https://doi.org/10.1002/prot.21221

8. Anthis NJ, Clore GM (2013) Sequence-specific determination of protein and peptide concentrations by absorbance at 205 nm. Protein Sci 22:851–858. https://doi.org/10.1002/pro.2253

9. Penner-Hahn JE (1999) X-ray absorption spectroscopy in coordination chemistry. Coordination Chemistry Reviews 190–192:1101–1123. https://doi.org/10.1016/S0010-8545(99)00160-5

10. Roe AL, Schneider DJ, Mayer RJ, et al (1984) X-ray absorption spectroscopy of iron-tyrosinate proteins. J Am Chem Soc 106:1676–1681. https://doi.org/10.1021/ja00318a021

11. Westre TE, Kennepohl P, DeWitt JG, et al (1997) A Multiplet Analysis of Fe K-Edge 1s → 3d Pre-Edge Features of Iron Complexes. J Am Chem Soc 119:6297–6314. https://doi.org/10.1021/ja964352a

12. Shu L, Chiou Y-M, Orville AM, et al (1995) X-ray absorption spectroscopic studies of the Fe(II) active site of catechol 2,3-dioxygenase. Implications for the extradiol cleavage mechanism. Biochemistry 34:6649–6659. https://doi.org/10.1021/bi00020a010

13. Hernick M, Gattis SG, Penner-Hahn JE, Fierke CA (2010) Activation of E. coli UDP-3-O-(R-3-hydroxymyristoyl)-N-acetylglucosamine deacetylase by Fe2+ yields a more efficient enzyme with altered ligand affinity. Biochemistry 49:2246–2255. https://doi.org/10.1021/bi902066t

14. Sarangi R, Hocking RK, Neidig ML, et al (2008) Geometric Structure Determination of N694C Lipoxygenase: A Comparative Near-Edge X-Ray Absorption Spectroscopy and Extended X-Ray Absorption Fine Structure Study. Inorg Chem 47:11543–11550. https://doi.org/10.1021/ic800580f

15. Rygula A, Majzner K, Marzec KM, et al (2013) Raman spectroscopy of proteins: a review. J Raman Spectroscopy 44:1061–1076. https://doi.org/10.1002/jrs.4335

16. Kitagawa T, Hirota S (2006) Raman Spectroscopy of Proteins. In: Handbook of Vibrational Spectroscopy. John Wiley & Sons, Ltd

17. Wright PG, Stein P, Burke JM, Spiro TG (1979) Resonance Raman spectra, excitation profiles and excited (iron .fwdarw. pyridine charge transfer) state geometry of bispyridine iron(II) heme. J Am Chem Soc 101:3531–3535. https://doi.org/10.1021/ja00507a018

18. Andrade GFS, Temperini MLA (2009) Identification of species formed after pyridine adsorption on iron, cobalt, nickel and silver electrodes by SERS and theoretical calculations. J Raman Spectroscopy 40:1989–1995. https://doi.org/10.1002/jrs.2354

19. Osman D, Martini MA, Foster AW, et al (2019) Bacterial sensors define intracellular free energies for correct enzyme metalation. Nat Chem Biol 15:241–249. https://doi.org/10.1038/s41589-018-0211-4

20. Hernick M (2012) Metalloenzymes: Native Co-factor or Experimental Artifact? Biochem Anal Biochem 01: https://doi.org/10.4172/2161-1009.1000e120

21. Gattis SG, Hernick M, Fierke CA (2010) Active Site Metal Ion in UDP-3-O-((R)-3-Hydroxymyristoyl)-N-acetylglucosamine Deacetylase (LpxC) Switches between Fe(II) and Zn(II) Depending on Cellular Conditions. J Biol Chem 285:33788–33796. https://doi.org/10.1074/jbc.M110.147173

22. Yunus AA, Lima CD (2009) Purification of SUMO conjugating enzymes and kinetic analysis of substrate conjugation. Methods Mol Biol 497:167–186. https://doi.org/10.1007/978-1-59745-566-4_11

23. Liebschner D, Afonine PV, Baker ML, et al (2019) Macromolecular structure determination using X-rays, neutrons and electrons: recent developments in Phenix. Acta Crystallogr D Struct Biol 75:861–877. https://doi.org/10.1107/S2059798319011471

24. Emsley P, Lohkamp B, Scott WG, Cowtan K (2010) Features and development of Coot. Acta Crystallogr D Biol Crystallogr 66:486–501. https://doi.org/10.1107/S0907444910007493

25. McCoy AJ, Grosse-Kunstleve RW, Adams PD, et al (2007) Phaser crystallographic software. J Appl Crystallogr 40:658–674. https://doi.org/10.1107/S0021889807021206

26. Meng EC, Goddard TD, Pettersen EF, et al (2023) UCSF ChimeraX: Tools for structure building and analysis. Protein Sci 32:e4792. https://doi.org/10.1002/pro.4792

27. Kuzmič P (1996) Program DYNAFIT for the Analysis of Enzyme Kinetic Data: Application to HIV Proteinase. Analytical Biochemistry 237:260–273. https://doi.org/10.1006/abio.1996.0238

28. Rao G, Pattenaude SA, Alwan K, et al (2019) The binuclear cluster of [FeFe] hydrogenase is formed with sulfur donated by cysteine of an [Fe(Cys)(CO)2(CN)] organometallic precursor. Proc Natl Acad Sci U S A 116:20850–20855. https://doi.org/10.1073/pnas.1913324116

29. George GN, Pickering IJ (2000) EXAFSPAK: A suite of computer programs for analysis of X-ray absorption spectra (documentation and program downloads)

Supplemental Information

The activation of the metal-containing regulatory protein NiaR from *Thermotoga maritima* by its effector, nicotinic acid

Wai Chung Dorothy Cheng*[,1], Yuxin Li*[,1,2], Maileen Nakashima[1], Pierre Moenne-Loccoz[3], Katherine Rush[1,3,4] and Arthur Glasfeld[1^]

[1]Department of Chemistry, Reed College, Portland, Oregon, USA 97202
[2]Present address: Department of Biochemistry, Duke University School of Medicine, Durham, NC, USA 27710
[3]Department of Chemical Physiology and Biochemistry, School of Medicine, Oregon Health and Science University, Portland, Oregon, USA 97239
[4]Present address: Department of Chemistry and Biochemistry, Auburn University, Auburn, Alabama, USA 36849
*These authors contributed to the manuscript equally.
^Corresponding author: glasfeld@reed.edu

Table S1. Metal content of purified TmNiaR samples. Each sample represents a separate purification trial.

Growth conditions	Detection Method	Protein conc. (μM)	[Fe] (μM)	[Zn] (μM)	%Fe	%Zn
Luria broth	ICP-MS	nd[a]	104	73	-	-
M9 + Fe, prep 1[b]	ICP-OES	70 ± 5	65.6 ± 0.2	5.8 ± 0.2	94	8
M9 + Fe, prep 2[b]	ICP-OES	60 ± 10	54.3 ± 0.1	0[c]	90	0

[a] The ICP-MS results for the LB-isolated TmNiaR reflect a single measurement. Protein concentration was was estimated by the bicinchoninic acid assay using albumin as a standard, but was not corrected to TmNiaR. Due to this we cannot rigorously determine metal occupancy, but the presence of significant concentrations of both Fe and Zn in this sample are clear.

[b]ICP-OES measurements were performed in triplicate and protein concentration was determined using amino acid analysis.

[c]A negative reading (-4 ± 4 μM) was obtained, indicating zinc concentration was below the limits of detection by our method.

Table S2 Vibrational frequencies (cm^{-1}) of pyridine-bound and NA-bound TmNiaR. Mode description and frequencies values for the iron(II)-dipyridine mesoporphyrin IX dimethyl ester complex ($(Py)_2Fe^{II}MP$) are from reference [17].

mode	*tm*NiaR(py)	$(py)_2Fe^{II}MP$	*tm*NiaR(py-d_5)	$(py\text{-}d_5)_2Fe^{II}MP$	*tm*NiaR(NA)	NA-d_4
1	1598	1597	1554	1557	1588	1557
2	*not obs.*	*not obs.*	1340	1340	*not obs.*	1342
3	1218	1216	892	899	1193	972
4	*1070*	*not obs.*	830	835	*not obs.*	863
5	*not obs.*	1044	*not obs.*	1021		1105
6	1005	1010	972	972	1031	998
7	622	635	598	609	641	621

a

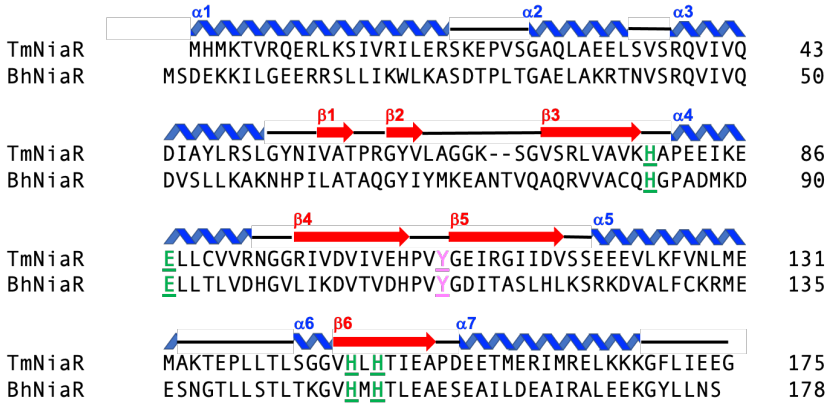

b

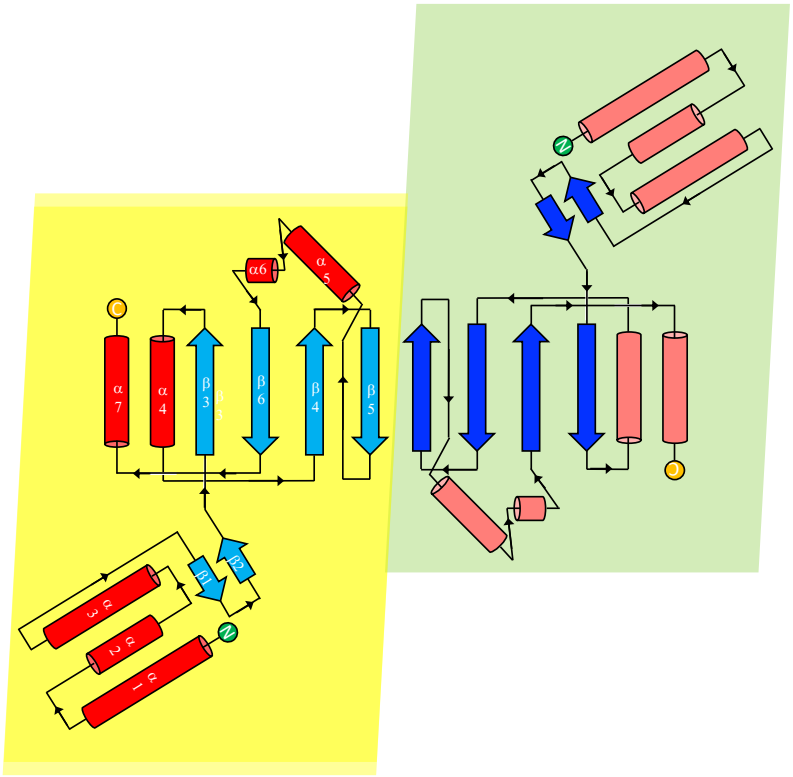

Fig. S1 Sequence and secondary structure map of NiaR: **a** Sequence alignment of TmNiaR with BhNiaR with secondary structure elements labeled as blue alpha helices and red beta strands. Metal-binding residues are underlined in green and a conserved tyrosine adjacent to the NA-binding site is underlined in magenta; **b** Secondary structure map of the TmNiaR dimer. The dimer interface is mediated by an 8-stranded beta sheet incorporating four strands from each subunit. The N-terminal winged helix-turn-helix DNA binding domains connect to the dimerization domains between beta-strands 2 and 3

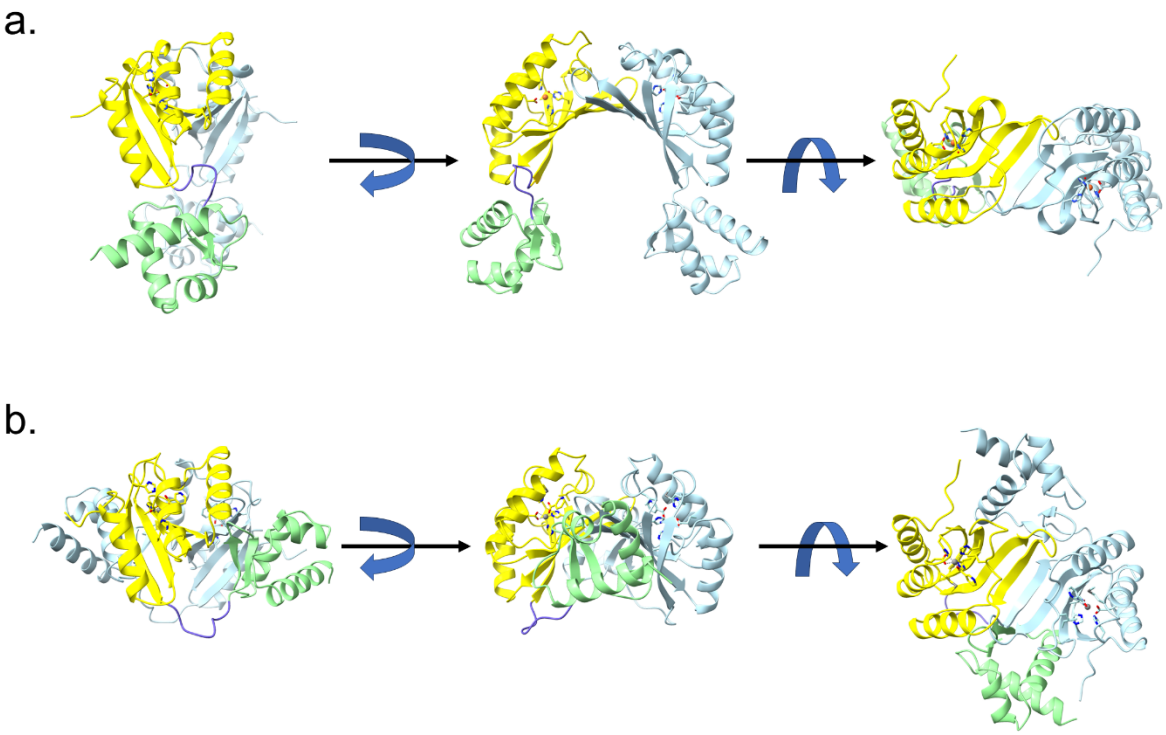

Fig. S2 Views of NiaR conformations: **a** Three orthogonal views of the TmNiaR dimer (PDB ID 1J5Y), colored as in Figure 1, showing the positions of the DNA-binding domains relative to the dimerization domains; **b** Equivalent views of BhNiaR (PDB ID 7CV2), with coloring as for TmNiaR.

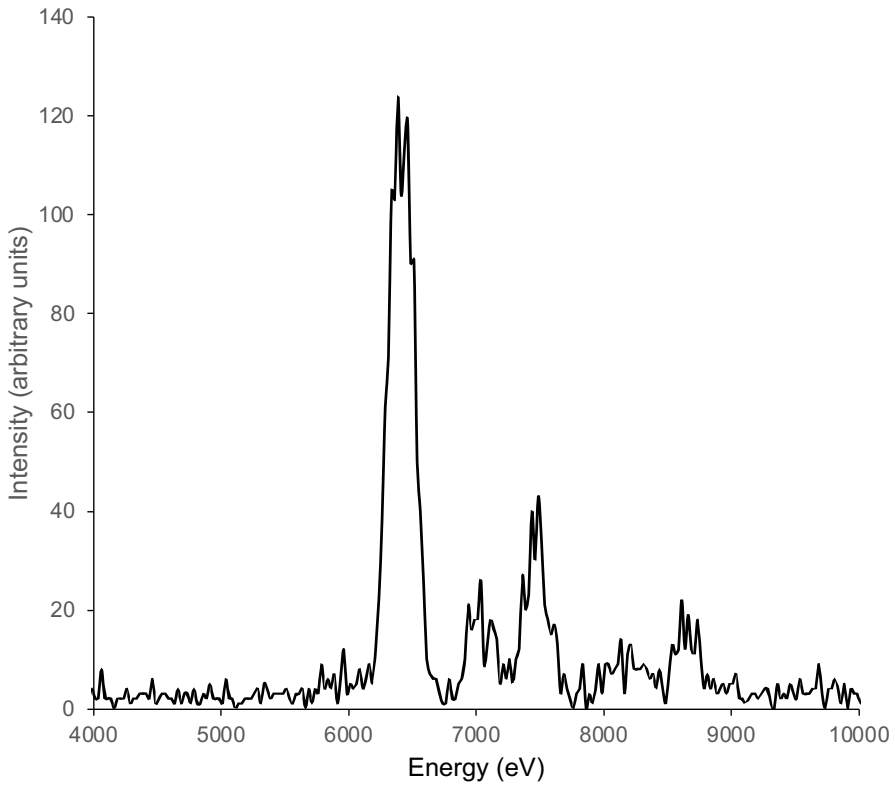

Fig. S3. X-ray fluorescence spectrum collected from NA-bound TmNiaR crystal irradiated with monochromatic synchrotron radiation (12.7 keV). The peak at roughly 6400 eV is assigned to iron (Fe K_{α} emission = 6404 eV). Smaller peaks at 6900 eV, 7500 eV and 8600 eV correspond to K_{α} emission resulting from cobalt, nickel and zinc respectively.

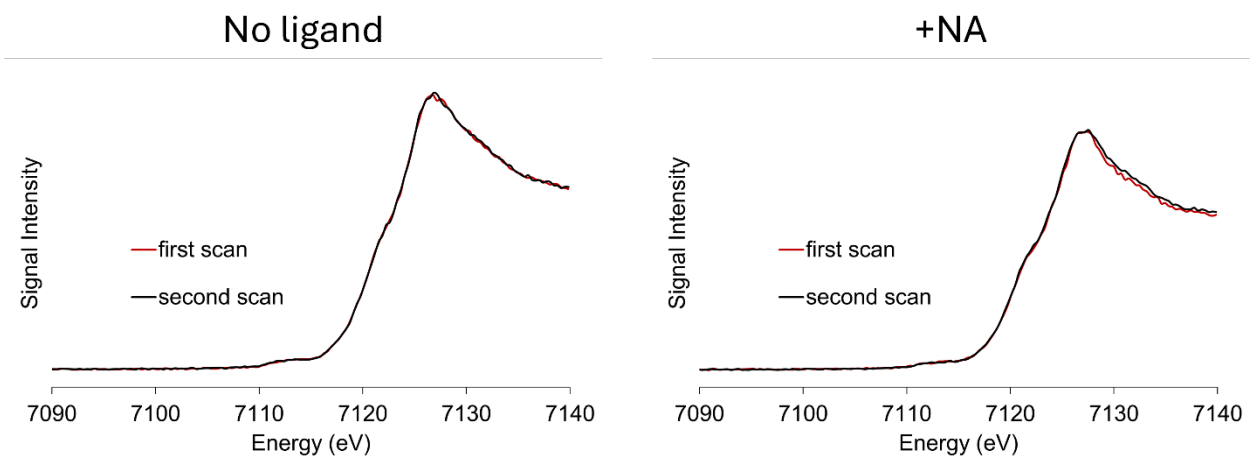

Fig. S4 Overlay of first (red line) and second (black line) Fe K-edge XANES scans of TmNiaR. No significant changes are seen that would indicate radiation damage affecting the spectra during data collection

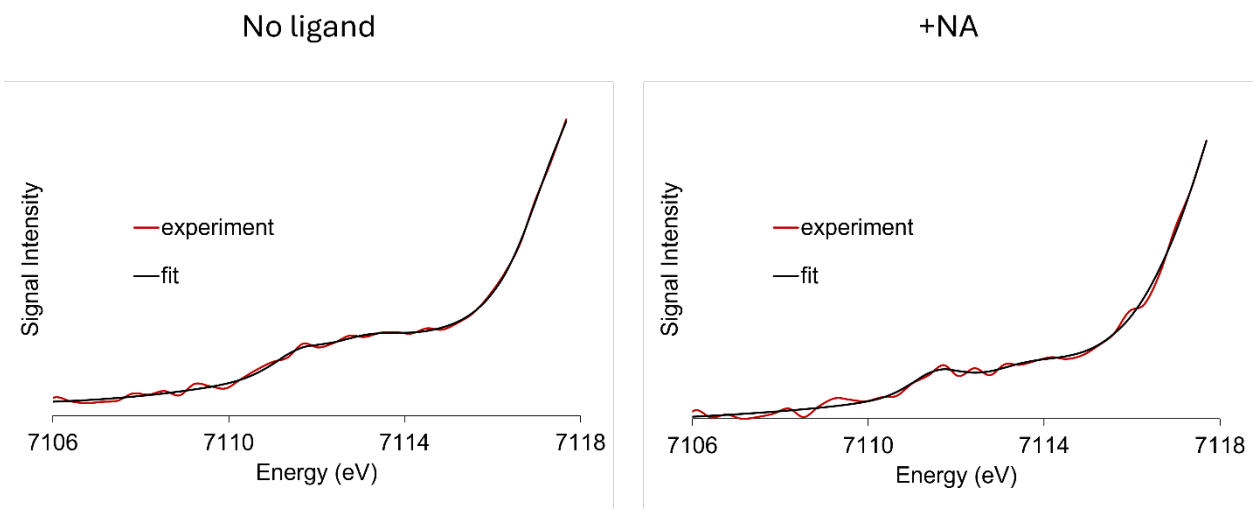

Fig. S5 Fits to experimental pre-edge data. In both cases, the fit includes a background function simulating the rising Fe K-edge and two pseudo-Voigt functions (50:50 Gaussian to Lorentzian ratio) modeling two pre-edge features centered at 7111.7 eV and 7113.1 eV (without NA) or 7113.4 eV (with NA).

a.

b.

c.

Fig. S6 Photos of TmNiaR in solution. **a** TmNiaR, as isolated from *E. coli* grown in minimal media containing ferric ammonium citrate and, **b** following the addition of NA. **c** Photomicrograph of a crystal of TmNiaR•Fe^{2+} bound to NA.

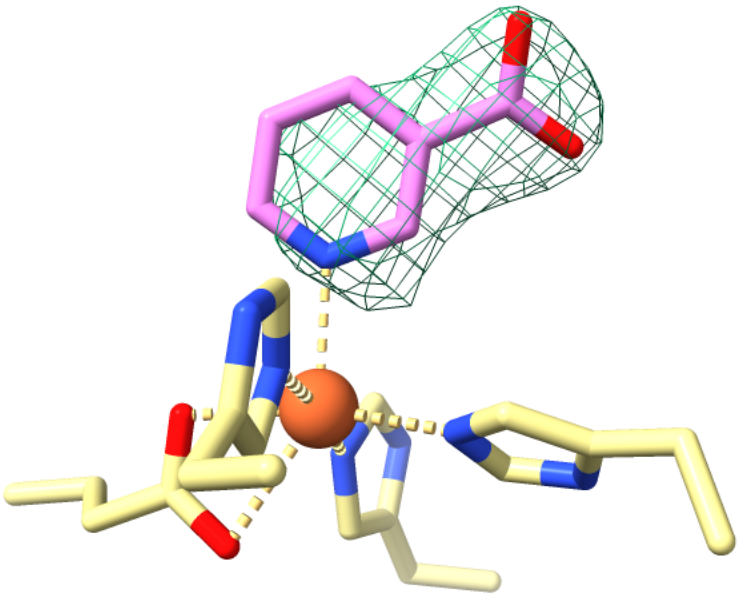

Fig. S7. Structure of the TmNiaR ligand binding site (as in Figure 2B) with NA modeled at 50% occupancy and the corresponding F_{obs}-F_{calc} map contoured at 5.5 σ. The strong density in the map indicates that NA exists at full occupancy in the crystals, rather than at half-of-sites as seen at lower NA concentrations in ligand binding studies.